Power Engineering and Engineering Thermophysics
https://www.acadlore.com/journals/PEET

Bilinear and Bicubic Interpolations for Image Presentation of Mechanical Stress and Temperature Distribution

Manikanta B. Pithani, Shubhashis Sanyal, Anuj K. Shukla*

Department of Mechanical Engineering, National Institute of Technology, 492010 Raipur, India

* Correspondence: Anuj K. Shukla (akshukla.me@nitrr.ac.in)

Received: 06-09-2022 **Revised:** 07-09-2022 **Accepted:** 07-23-2022

Citation: M. B. Pithani, S. Sanyal, and A. K. Shukla, "Bilinear and bicubic interpolations for image presentation of mechanical stress and temperature distribution," *Power Eng. Eng Thermophys.*, vol. 1, no. 1, pp. 8-18, 2022. https://doi.org/10.56578/peet010103.

Abstract: Bilinear and bicubic interpolations were often used in digital elevation models (DEMs), image scaling, and image restoration, with the aid of spatial transform techniques. This paper resorts to bilinear and bicubic interpolations, along with the spatial transform of images, to present the temperature distribution on a plate with a circular hole. The Dirichlet boundary conditions were applied, a rectangular grid was created, and the nodal values were calculated using the finite difference method (FDM). These methods were also employed to represent the mechanical stress distribution on a plate with a circular hole, under the presence of uniaxial stress. In this case, the nodal values were calculated using the analytical method. Experimental results show that bicubic interpolation generated continuous contours, while bilinear interpolation had a discontinuity in some cases. The results were comparative to images for similar cases when solved through ANSYS.

Keywords: Bilinear interpolation; Bicubic interpolation; Spatial transform; Temperature distribution; Plate with a circular hole

1. Introduction

With the help of interpolation techniques, many software applications eliminate the problem of image pixelation while zooming. There are various readily available interpolation techniques, ranging from single interpolation to multivariate interpolation. When it comes to image scaling, resizing and restoration, bilinear and bicubic interpolation methods were commonly and widely used in many fields.

Using bilinear and Brownian interpolations, Polidori and Chorowicz [1] analyzed digital elevation models (DEMs), and compared the two methods on topographic and hydrographic surfaces, under the criteria of maximum deviation and texture quality. Similarly, Shi et al. [2] modelled the analytical form for the accuracy of DEMs, and measured the accuracy by resolution and terrain slope. Zhang et al. [3] adopted four surface interpolation techniques, namely, inverse distance weighted interpolation, ordinary kriging interpolation, radial basis function (RBF) interpolation, and cubic spline function interpolation, to plot the contours of the shockwave overpressure field of a 7.62mm calibre naval gun, and obtained the relevant values with a sensor array based on the polar coordinates. The interpolated data were cross-validated with mean relative error, mean absolute error, and root mean square error. Leng et al. [4] proposed a registration-based image interpolation approach, which comprises image registration and intensity interpolation. The images were registered with the B-spline vector-based function. After that, the intensity was derived through bilinear interpolation or bicubic interpolation.

Drawing on RBF interpolation, Wang et al. [5] put forward a new sub-pixel mapping method, and applied the method on remote sensing images, with the coarse image data as input. Xia et al. [6] applied bilinear interpolation, bicubic interpolation and B-spline interpolation to parallel phase-shifting digital holography, and compared the results by the quality of the reconstructed images. Through fuzzy error interpolation, Bai and Zhuang [7] identified and compensated the position error of the end-effector of a robot, and compared the results of fuzzy error interpolation with those of bilinear and cubic spline interpolations through simulation. Gribbon and Bailey [8] introduced bilinear interpolation to correct lens distortion, which is a real-time problem with the input coordinates of the pixels following a curved path. The coordinates were retrieved by forward and inverse mapping between

distorted and corrected images.

Bozorgmanesh et al. [9] searched for the nanoparticle size in rapid expanding supercritical fluids, using Lagrangian bivariate interpolation, and assured that the powder generated by pharmaceutical industries have uniform properties. Bhattacharjee and Majumder [10] developed two algorithms on multivariate interpolation. One of them consumes a relatively long time yet yields accurate results, while the other works fast but lacks accuracy. Inspired by the finite element method, Gopalakrishnan and Korttom [11] developed an algorithm for contour plot and interpolation of regularly and irregularly distributed field data. Eltuhamy et al. [12] innovatively utilized infrared thermography image analysis to detect and predict the fault features of CIGS PV modules. The novelty of their technique manifests in the utilization and analysis of the captured thermal images. Senalp and Ceylan [13] drew thermal images of neonates using a high-resolution thermal camera. These images were then downscaled and subjected to super-resolution methods, using different data sets based on deep learning.

The present work resorts to bilinear and bicubic image interpolations to clarify the temperature distribution on a rectangular plate with a circular hole. Multiple techniques were employed to mark the contours of the stress intensity over the said plate, in the light of the stress concentration factor. This factor has been considered by several researchers [14] based on diameter to width ratio. Both bicubic and bilinear interpolations were simulated on MATLAB with the same number of iterations. The simulation results were compared with those of FEM on ANSYS software, Mechanical APDL Student version 2021 R2.

2. Methodology

Image interpolation using different techniques is an active research area involving researchers from many different countries and regions. In the present work, bilinear and bicubic interpolations are compared in different scenarios, such as irregular geometry and the combination between Neumann and Dirichlet boundary conditions, which are considered to demonstrate the discontinuities in the contours.

2.1 Image Restoration by Spatial Transform

Figure 1 provides a representation of image interpolation. Each node represents a pixel, and the nodal value is assigned to the corresponding pixel. The pixel value is illustrated by a significant color (Figure 1(a)). The spatial transform is explained in Figure 1(b): each grid is expanded, and null pixels are added between the initial pixels. The addition is realized through bilinear and bicubic interpolations (Figure 1(c)), and only takes one single iteration. To obtain the contours of the data, however, more iterations are required until the high-resolution image is acquired.

For the rectangular plate with a circular hole, the irregular boundaries can be addressed with the help of an equation for irregular geometry. As shown in Figure 2, the pixel values falling in the equation of that geometry must be removed [15].

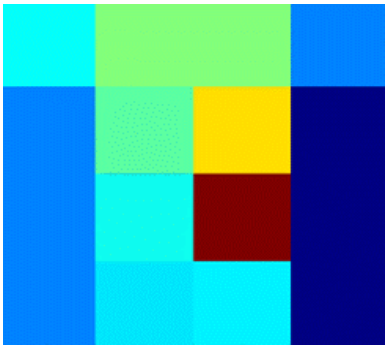

(a) Initial nodal values as pixels

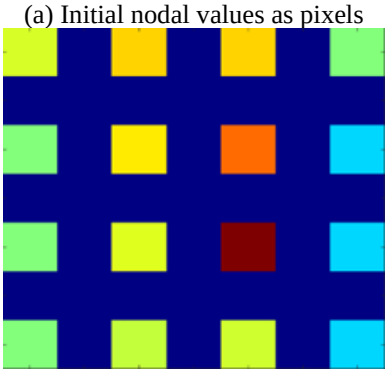

(b) Spatial transform

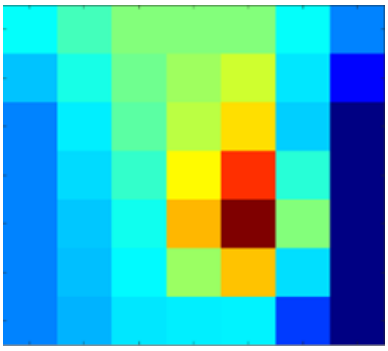

(c) Interpolated image

Figure 1. Representation of image interpolation

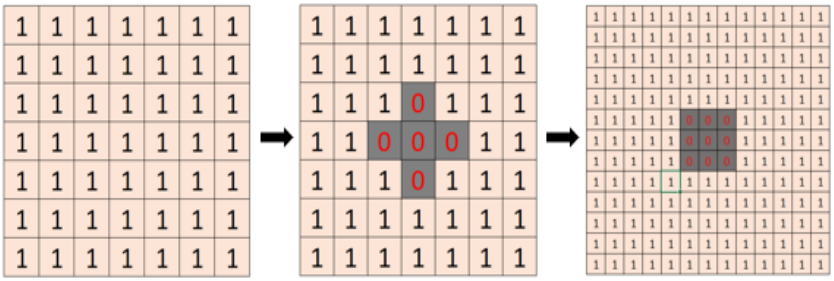

Figure 2. Creating irregular geometry in meshed grid

2.2 Bilinear Interpolation

As shown in Figure 3, the bilinear surface can be represented by:

$$ff(x,y) = a_0 + a_1 x + a_2 y + a_3 xy \tag{1}$$

Four points are required to find the four coefficients of the equation by solving the simultaneous Eq. (2) from the given points:

$$\begin{bmatrix} f(0,0) \\ f(1,0) \\ f(0,1) \\ f(1,1) \end{bmatrix} = \begin{bmatrix} 1 & 0 & 0 & 0 \\ 1 & 1 & 0 & 0 \\ 1 & 0 & 1 & 0 \\ 1 & 1 & 1 & 1 \end{bmatrix} \begin{bmatrix} a_{00} \\ a_{10} \\ a_{01} \\ a_{11} \end{bmatrix} \tag{2}$$

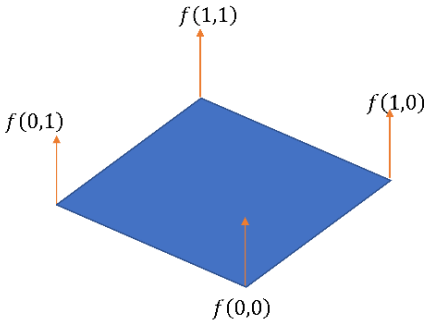

Figure 3. Bilinear surface

After obtaining the coefficients (a_0, a_1, a_2, a_3) of Eq. (1), the bilinear interpolation can be simplified by computing the midpoint values with the mean values from the four neighbour points (f(0,0), f(1,0), f(0,1), f(1,1)) (Figure 4).

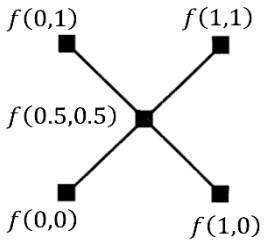

Figure 4. Bilinear interpolation using mean values

2.3 Bicubic Interpolation

As shown in Figure 5, the bicubic surface can be represented with Eq. (3) with sixteen nodal values equidistant from each other:

$$f(x,y) = a_{00} + a_{10}x + a_{01}y + a_{11}xy + a_{20}x^2 + a_{02}y^2 + a_{21}x^2y + a_{12}y^2x + a_{22}x^2y^2 + a_{30}x^3 + a_{03}y^3 + a_{31}x^3y^1 + a_{13}x^1y^3 + a_{32}x^3y^2 + a_{23}x^2y^3 + a_{33}x^3y^3 \quad (3)$$

Substituting the obtained coefficients of Eq. (3), sixteen equations are framed by substituting sixteen nodal values in the bicubic equation, and the simultaneous equations represented by Eq. (4) are solved using Gauss Seidel or Gauss Jordan methods:

$$[f]_{16x1} = [X]_{16x16}\,[a]_{16x1} \quad (4)$$

The results of Eq. (4) are rearranged to form the Lagrange bivariate interpolation:

$$f(x,y) = \sum_{i=0}^{3}\sum_{j=0}^{3} f(x_i,y_j).L_{ij}(x,y) \quad (5)$$

$$L_{ij}(x,y) = L_i(x).L_j(y)$$

where,

$$L_i(x) = \prod_{s=0,s\neq i}^{n}\left(\frac{x-x_s}{x_i-x_s}\right)$$

$$L_j(y) = \prod_{s=0,s\neq j}^{m}\left(\frac{y-y_s}{y_j-y_s}\right)$$

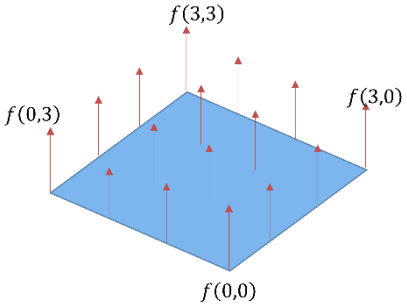

Figure 5. Bicubic surface

3. Results and Discussion

Bilinear and bicubic interpolation methods are only applicable to two-dimensional (2D) problems. In this section, their results are evaluated and compared in different cases.

3.1 Temperature Distribution on Plate with Circular Hole

A circular hole was added to form an irregular grid on the rectangular plate. This paper takes a similar problem with boundary conditions, yet without a hole, as a reference [16]. Boundary conditions were applied to maintain the constant temperatures on the four edges of the rectangular plate. Figure 6 shows the constant temperature on the boundary of the circular hole. The interior nodal values can be calculated by the Laplacian equation:

$$\frac{d^2T}{dx^2} + \frac{d^2T}{dy^2} = 0 \tag{6}$$

The finite difference method can be represented by:

$$\frac{T_{i+1,j} - 2T_{i,j} + T_{i-1,j}}{\Delta x^2} + \frac{T_{i,j+1} - 2T_{i,j} + T_{i,j-1}}{\Delta y^2} = 0 \tag{7}$$

The four nodes near irregular boundaries can be obtained by substituting Eqns. (8a) into Eq. (6):

$$\frac{d^2T}{dx^2} = \frac{2}{\Delta x^2}\left[\frac{T_{i-1,j} - T_{i,j}}{\alpha_1(\alpha_1 + \alpha_2)} + \frac{T_{i+1,j} - T_{i,j}}{\alpha_2(\alpha_1 + \alpha_2)}\right] \tag{8a}$$

$$\frac{d^2T}{dy^2} = \frac{2}{\Delta y^2}\left[\frac{T_{i,j-1} - T_{i,j}}{\beta_1(\beta_1 + \beta_2)} + \frac{T_{i,j+1} - T_{i,j}}{\beta_2(\beta_1 + \beta_2)}\right] \tag{8b}$$

The width (b) = 30mm, height (b) = 30mm, and hole radius (a) = 5mm.

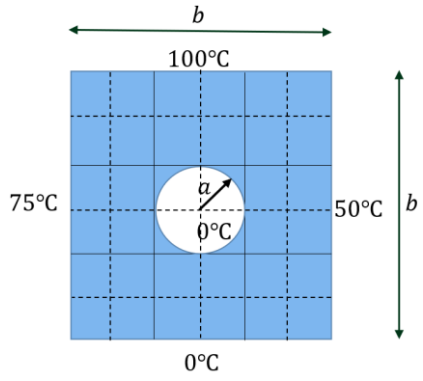

(a) 6×6 grid

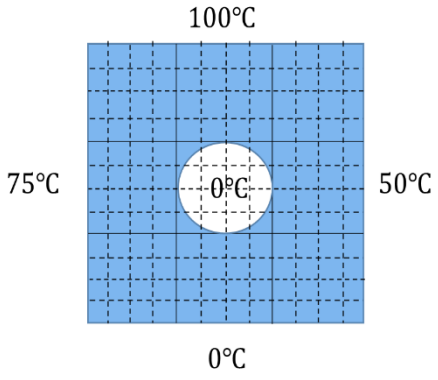

(b) 12×12 grid

Figure 6. Rectangular plate with circular hole with a constant temperature

As shown in Figure 6(a), the grid of the size 6×6 contains fewer nodes to represent the circular boundary. Thus, it was further divided to obtain a 12×12 grid (Figure 6(b)). For the modified grid, there are sixteen nodes falling around the boundary of the circular hole. These are sufficient to represent the boundary of a circular hole in the spatial transform of an image. There are a total of 121 interior nodes in the modified grid (Figure 6(b)), after

neglecting the 13 nodes as boundary conditions (4 nodes on circumference, and 9 nodes at center). These interior nodes form a 108×108 matrix, which can be solved by Gauss Seidel or Gauss Jordan methods. Then, both bilinear and bicubic interpolation techniques were applied on the calculated data.

Firstly, simulation results were obtained using MatLab programs for bilinear and bicubic interpolations, While the irregular geometries were represented with an equation in the code. Some discontinuous contours were observed in the bilinear interpolation, as shown in Figures 7(a) and (b).

Bicubic interpolation yielded smoother and more accurate contours than bilinear interpolation. The results of the two interpolations were compared with those obtained by the finite element method computed using ANSYS (Mechanical APDL version 2021 R2), as shown in Figure 7(c).

According to Figures 7(a)-(c), there were discontinuities in the bilinear interpolation contours, and the results of both interpolations were comparable to the ANSYS results.

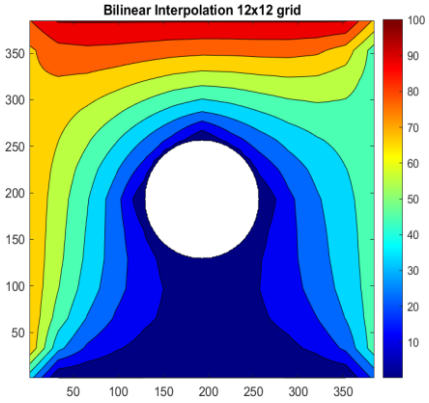

(a) Bilinear interpolation

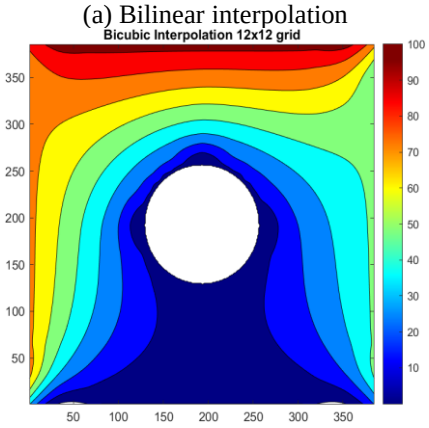

(b) Bicubic interpolation

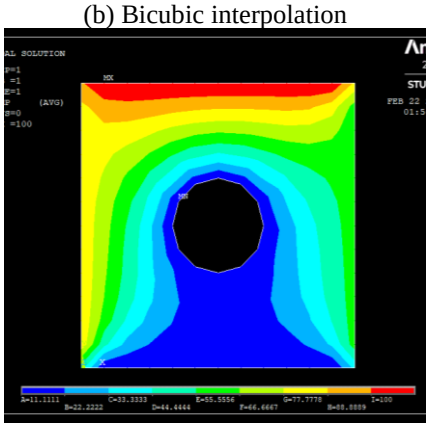

(c) ANSYS results

Figure 7. Temperature distribution on rectangular plate with circular hole

3.2 Stress Distribution on Flat Plate with Circular Hole

As shown in Figure 8, a uniaxial load was applied on a flat plate with a circular hole, which is represented as a 12×12 grid. Nodal values were calculated as follows:

The stress along the radial direction can be solved by:

$$\sigma_{rr} = \frac{\sigma}{2}\left(1 - \frac{a^2}{r^2}\right) + \frac{\sigma}{2}\left(1 - \frac{a^2}{r^2}\right)\left(1 - \frac{3a^2}{r^2}\right) cos\, 2\theta \tag{9}$$

The circumferential stress can be solved by:

$$\sigma_{\theta\theta} = \frac{\sigma}{2}\left(1 + \frac{a^2}{r^2}\right) - \frac{\sigma}{2}\left(1 + \frac{3a^4}{r^4}\right) cos\, 2\theta \tag{10}$$

The shear stress can be solved by:

$$\sigma_{r\theta} = -\frac{\sigma}{2}\left(1 - \frac{a^2}{r^2}\right)\left(1 + \frac{3a^2}{r^2}\right) sin\, 2\theta \tag{11}$$

The above equation was developed from the airy stress function and substituting those values in von-Mises equivalent stress:

$$\sigma_{eq} = \sqrt{\frac{(\sigma_1 - \sigma_2)^2}{2} + \frac{(\sigma_2 - \sigma_3)^2}{2} + \frac{(\sigma_1 - \sigma_3)^2}{2}} \tag{12}$$

The bilinear and bicubic interpolations were applied after obtaining the data for all nodes, using $\boldsymbol{r_{ij}}$ to represent the stress contours. The width (b) = 30mm, height (b) = 30mm, hole radius (a) = 5mm, thickness (t) = 1mm, and applied load (σ) = 166.67 kPa.

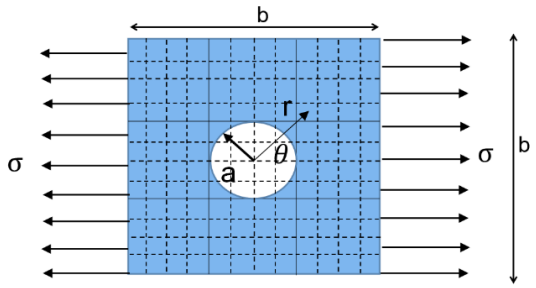

Figure 8. Flat plate with circular hole under uniaxial loading (12x12 Grid)

The irregular geometry would result in the localization of high stresses, i.e., stress concentration. Considering this phenomenon, stress concentration factors were used to calculate the equivalent stresses at nodal points in Figure 8. These factors were taken directly from the work of Nagpal et al. [14], and have been considered by many researchers. In addition, the results obtained without taking account of the stress concentration factors (Figures 9(a), (b) and (c)). The results of both bilinear and bicubic interpolations were both smaller than those of ANSYS. This is the result of the effect of stress concentration factors.

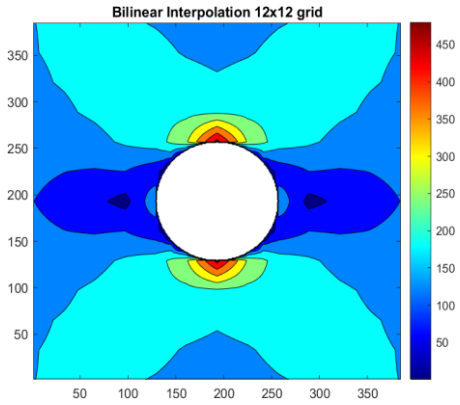

(a) Bilinear interpolation results

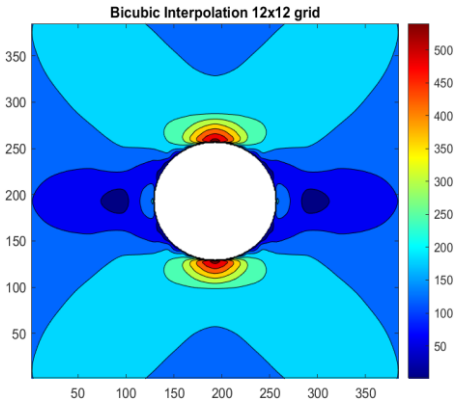

(b) Bicubic interpolation results

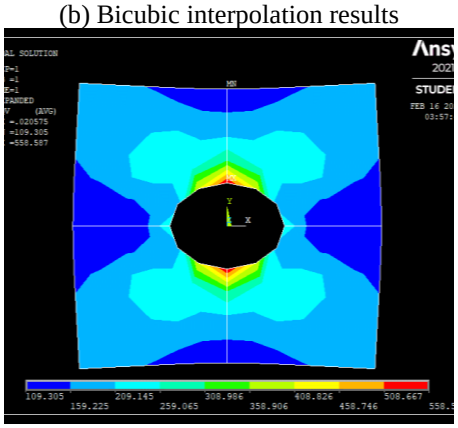

(c) ANSYS results

Figure 9. Stress contours for uniaxial load applied on flat plate with circular hole

3.3 Temperature Distribution on Rectangular Plate with Insulate Edge

Finally, a rectangular plate was maintained with constant temperatures on three edges, and with the remaining edge insulated, as shown in Figure 10. The example was taken from Chapra and Canale [16]. The results were displayed to show the difference between bilinear and bicubic interpolations, with the aid of temperature contours. The purpose is to illustrate the impact of the temperature gradients using both bilinear and bicubic interpolations. This problem was also solved by the Laplacian equation Eq. (6) with finite difference scheme Eq. (7).

The width (b) = 30mm, height (b) = 30mm, and distance (h) = 10mm.

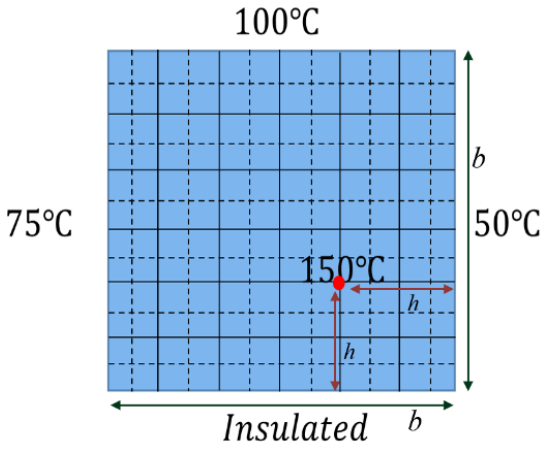

Figure 10. Rectangular plate with boundary condition

As stated above, the example from Chapra and Canale [16] was cited to check the discontinuities in the contours, as well as the difference between both the interpolation methods. As shown in Figures 11, bilinear interpolation yielded discontinuous contours, while bicubic interpolation provided smooth contours with accurate results.

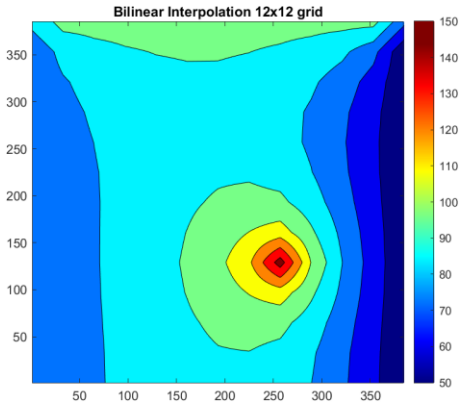

(a) Bilinear interpolation

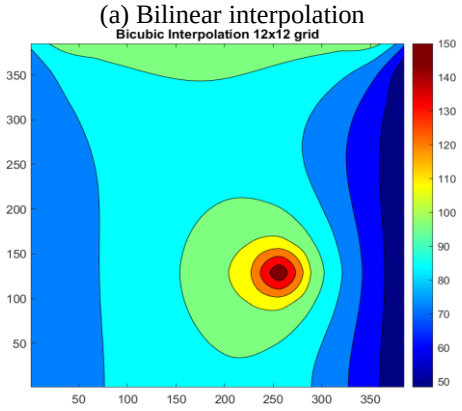

(b) Bicubic interpolation

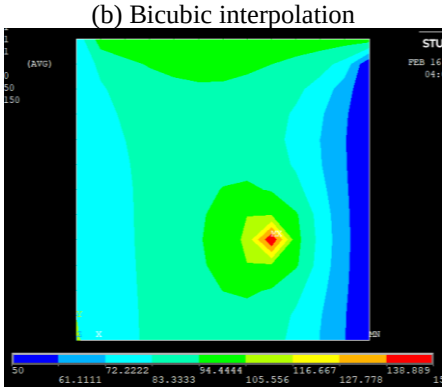

(c) ANSYS results

Figure 11. Temperature distribution on rectangular plate with insulate edge

4. Conclusions

Bilinear and bicubic interpolations were applied after the spatial image transform on the original data of calculated nodal values. The present results show that bilinear interpolation yields discontinuous contours, failing to capture the variation in some data points. By contrast, the bicubic interpolation provides smooth contours. In general, grids can be taken such that the nodes fall on maximum or minimum values and irregular boundaries. Besides, bilinear interpolation offers an option to make the computations faster apart from neglecting the accuracy in results. Bicubic methods can be applied where the accuracy of results plays an important role, at the cost of more computation time.

Data Availability

The data used to support the research findings are available from the corresponding author upon request.

Conflicts of Interest

The authors declare no conflict of interest.

References

[1] L. Polidori and J. Chorowicz, "Comparison of bilinear and Brownian interpolation for digital elevation models," *ISPRS J. Photogramm.*, vol. 48, no. 2, pp. 18-23, 1993. https://doi.org/10.1016/0924-2716(93)90036-M.

[2] W. Shi, B. Wang, and Y. Tian, "Accuracy analysis of digital elevation model relating to spatial resolution and terrain slope by bilinear interpolation," *Math. Geosci.*, vol. 46, no. 4, pp. 445-481, 2014. https://doi.org/10.1007/s11004-013-9508-8.

[3] Y. Zhang, T. Han, H. Liu, X. Wang, and E. Zhang, "Cooperation of the spatial interpolation algorithm for the contour map of the shockwave overpressure field," *J. Eng. Sci. Technol. Rev.*, vol. 10, no. 6, pp. 104-110, 2017. https://doi.org/10.25103/jestr.106.14.

[4] J. Leng, G. Xu, and Y. Zhang, "Medical image interpolation based on multi-resolution registration," *Comput. Math Appl.*, vol. 66, no. 1, pp. 1-18, 2013. https://doi.org/10.1016/j.camwa.2013.04.026.

[5] Q. Wang, W. Shi, and P. M. Atkinson, "Sub-pixel mapping of remote sensing images based on radial basis function interpolation," *ISPRS J Photogramm.*, vol. 92, pp. 1-15, 2014. https://doi.org/10.1016/j.isprsjprs.2014.02.012.

[6] P. Xia, T. Tahara, T. Kakue, Y. Awatsuji, K. Nishio, S. Ura, T. Kubota, and O. Matoba, "Performance comparison of bilinear interpolation, bicubic interpolation, and b-spline interpolation in parallel phase-shifting digital holography," Opt. Rev., vol. 20, no. 2, pp. 193-197, 2013. https://doi.org/10.1007/s10043-013-0033-2.

[7] Y. Bai and H. Zhuang, "On the comparison of bilinear, cubic spline, and fuzzy interpolation techniques for robotic position measurements," *IEEE Trans. Instrum. Meas.*, vol. 54, no. 6, pp. 2281-2288, 2005. https://doi.org/10.1109/TIM.2005.858563.

[8] K. T. Gribbon and D. G. Bailey, "A novel approach to real-time bilinear interpolation," In Second IEEE International Workshop on Electronic Design, Test and Applications, (DELTA 2004), Perth, WA, Australia, January 28-30, 2004, IEEE, pp. 126-131.

[9] A. R. Bozorgmanesh, M. Otadi, A. A. S. Kordi, F. Zabihi, and M. B. Ahmadi, "Lagrange two-dimensional interpolation method for modeling nanoparticle formation during RESS process," *In Int. J. Industrial Mathematics*, vol. 1, no. 2, pp. 175-181, 2009.

[10] G. P. Bhattacharjee and K. L. Majumder, "Multivariate interval interpolation," *J. Comput. Appl. Math*, vol. 4, no. 4, pp. 295-300, 1978. https://doi.org/10.1016/0771-050X(78)90029-3.

[11] T. C. Gopalakrishnan and M. Korttom, "An algorithm for contouring and interpolation of data using bilinear finite elements," *Finite Elem. Anal. Des.*, vol. 14, no. 1, pp. 37-54, 1993. https://doi.org/10.1016/0168-874X(93)90077-4.

[12] R. A. Eltuhamy, M. Rady, K. H. Ibrahim, and H.A. Mahmoud, "Novel features extraction for fault detection using thermography characteristics and IV measurements of CIGS thin-film module," *Instrum. Mesure Metrologie*, vol. 19, no. 5, pp. 311-325, 2020. https://doi.org/10.18280/i2m.190501.

[13] F. M. Senalp and M. Ceylan, "Deep learning based super resolution and classification applications for neonatal thermal images," *Trait. Signal*, vol. 38, no. 5, pp. 1361-1368, 2021. https://doi.org/10.18280/ts.380511.

[14] S. Nagpal, N. Jain, and S. Sanyal, "Stress concentration and its mitigation techniques in flat plate with singularities-a critical review," *Eng. J.*, vol. 16, no. 1, pp. 1-15, 2012. https://doi.org/10.4186/ej.2012.16.1.1.

[15] "Rumpf," EMPossible, 2020, https://empossible.net/academics/emp4301_5301/.

[16] S. C. Chapra and R. P. Canale, Numerical Methods for Engineers, Eighth Edition, McGraw-Hill Education, 2015.

Nomenclature

L_{ij}	Lagrangian interpolation function
n	No.of terms in x-direction
m	No.of terms in y-direction
x_s	x-value at point s
x_i	x-value at point i
y_j	y-value at point j
y_s	y-value at point s
T	Temperature
T_{ij}	Temperature at point (i, j)
r_{ij}	Radial distance to point (i, j)
b	Width / height of rectangular plate
a	Radius of circular hole

h	Distance of temperature source

Greek symbols

α	x-distance from irregular boundary
β	y-distance from irregular boundary
σ	Stress kPa

Subscripts

rr	Radial direction
$\Theta\Theta$	Circumferential direction
rΘ	Tangential direction
eq	Equivalent stress